# The nature of X-ray-absorbed quasi-stellar objects

M. J. Page,[1]⋆ F. J. Carrera,[2] J. A. Stevens,[3] J. Ebrero[4] and A. J. Blustin[1,5]

[1]*Mullard Space Science Laboratory, University College London, Holmbury St Mary, Dorking, Surrey RH5 6NT*
[2]*Instituto de Física de Cantabria (CSIC–Universidad de Cantabria), 39005 Santander, Spain*
[3]*Centre for Astrophysics Research, University of Hertfordshire, College Lane, Hertfordshire AL10 9AB*
[4]*SRON National Institute for Space Research, Sorbonnelaan 2, 3584 CA Utrecht, the Netherlands*
[5]*Institute of Astronomy, University of Cambridge, Madingley Road, Cambridge CB3 0HA*

## ABSTRACT

There exists a significant population of broad line, $z \sim 2$ quasi-stellar objects (QSOs) which have heavily absorbed X-ray spectra. Follow-up observations in the submillimetre show that these QSOs are embedded in ultraluminous starburst galaxies, unlike most unabsorbed QSOs at the same redshifts and luminosities. Here we present X-ray spectra from *XMM–Newton* for a sample of five such X-ray-absorbed QSOs that have been detected at submillimetre wavelengths. We also present spectra in the rest-frame ultraviolet from ground-based telescopes. All the five QSOs are found to exhibit strong C IV absorption lines in their ultraviolet spectra with equivalent width $>5$ Å. The X-ray spectra are inconsistent with the hypothesis that these objects show normal QSO continua absorbed by low-ionization gas. Instead, the spectra can be modelled successfully with ionized absorbers, or with cold absorbers if they possess unusually flat X-ray continuum shapes and unusual optical to X-ray spectral energy distributions. We show that the ionized absorber model provides the simplest, most self-consistent explanation for their observed properties. We estimate that the fraction of radiated power that is converted into kinetic luminosity of the outflowing winds is typically $\sim 4$ per cent, in agreement with recent estimates for the kinetic feedback from QSOs required to produce the $M$–$\sigma$ relation, and consistent with the hypothesis that the X-ray-absorbed QSOs represent the transition phase between obscured accretion and the luminous QSO phase in the evolution of massive galaxies.

**Key words:** galaxies: active – galaxies: evolution – galaxies: formation – X-rays: galaxies.

## 1 INTRODUCTION

The prevalence of black holes in present-day galaxy bulges, and the proportionality between black hole and spheroid mass (Magorrian et al. 1998; Merritt & Ferrarese 2001), implies that the formation of the stars in a present-day galaxy spheroid was fundamentally connected to the growth of the black hole as an active galactic nucleus (AGN). In fact, an evolutionary connection between the star-forming and AGN-dominated phases of galaxies has long been posited (e.g. Sanders et al. 1988).

It is now known that a significant fraction of cosmic star formation took place in submillimetre galaxies (SMGs): dusty, ultraluminous and highly obscured galaxies at high redshift (Smail, Ivison & Blain 1997; Hughes et al. 1998). Although some distant QSOs have been detected as submillimetre sources in pointed observations (e.g. McMahon et al. 1999; Page et al. 2001a), the overlap

between the QSO and SMG populations is relatively small (Fabian et al. 2000; Severgnini et al. 2000; Almaini et al. 2003; Waskett et al. 2003; Lutz et al. 2010). In an attempt to uncover the relationship between quasi-stellar objects (QSOs) and SMGs, Page et al. (2004) observed matched samples of X-ray-absorbed and unabsorbed QSOs at 850 μm with Submillimetre Common-User Bolometer Array (SCUBA). These observations revealed a remarkable dichotomy in the submillimetre properties of these two groups of sources: a substantial fraction ($\sim 50$ per cent) of X-ray-absorbed QSOs are SMGs, while X-ray-unabsorbed (i.e. normal) QSOs are not. This suggests that the two types are linked by an evolutionary sequence in which the X-ray-absorbed QSOs correspond to the transition between the main star-forming phase and the QSO phase of a massive galaxy (Page et al. 2004; Stevens et al. 2005; Coppin et al. 2008). The space density and luminosities of the X-ray-absorbed QSOs indicate that this transitional phase is relatively brief, $\sim 15$ per cent of the duration of the luminous QSO phase.

However, the physical driver for this transition between obscured star-forming galaxy and luminous QSO is unknown. Furthermore,

⋆E-mail: mjp@mssl.ucl.ac.uk

the nature of the X-ray absorption in the X-ray-absorbed QSOs remains puzzling. These objects are characterized by hard, absorbed X-ray spectra, but they have optical/ultraviolet (UV) spectra which are typical for QSOs, with broad emission lines and blue continua. Assuming that their hard X-ray spectral shapes result from photoelectric absorption from cold material with solar abundances, the column densities are of the order of $10^{22}$ cm$^{-2}$. The X-ray absorption could be due to gas located within the AGN structure, or from more distant material in the host galaxy. Wherever the absorber is located, it appears to contain very little dust: for a Galactic gas/dust ratio, the rest-frame UV spectra would be heavily attenuated by such large columns of material.

Therefore in order to investigate the X-ray absorption in these objects, we have obtained deep (50–100 ks) *XMM–Newton* observations of five X-ray-absorbed QSOs from our sample of hard-spectrum *ROSAT* sources (Page, Mittaz & Carrera 2001b) that were detected as powerful submillimetre sources with SCUBA (Page et al. 2001a; Stevens et al. 2005).

Throughout this paper, we assume $H_0 = 70$ km s$^{-1}$ Mpc$^{-1}$, $\Omega_{\rm m} = 0.3$ and $\Omega_\Lambda = 0.7$. We define a power-law spectrum such that $f_\nu \propto \nu^{-\alpha}$; we assign the energy index $\alpha$ the subscript X when it refers to the X-ray spectral slope, O when it refers to the optical/UV spectral slope and OX when it refers to the optical to X-ray spectral slope.

## 2 OBSERVATIONS AND DATA REDUCTION

### 2.1 Optical spectra

RX J005734 was observed on 1998 November 22, with the European Southern Observatory (ESO) 3.6-m telescope at La Silla, Chile. The EFOSC 2 spectrograph was used with the 5000-Å blaze, 300 lines mm$^{-1}$ grism covering the wavelength range 3800–8000 Å, with a spectral resolution of 20-Å full width at half-maximum (FWHM).

RX J094144, RX J121803 and RX J163308 were observed on 1998 March 3–5 with the William Herschel Telescope at the Observatorio del Roque de los Muchachos, La Palma. The dual arm ISIS spectrograph was used with the 5400-Å dichroic, the R158R grating on the red arm and the R300B grating on the blue arm. The two ISIS arms combined give continuous coverage of the wavelength range 3200–8100 Å with resolution of 5-Å FWHM in the blue and 9-Å FWHM in the red.

In both observing runs, arc-lamp spectra and observations of spectrophotometric standard stars were taken for wavelength and flux calibration. The spectra were reduced and calibrated using standard routines in IRAF.

RX J124913 was not observed because it is a well-known broad absorption line QSO (BALQSO) with optical spectra available in the literature; the spectrum shown in Fig. 1 is taken from Junkkarinen, Burbidge & Smith (1987).

### 2.2 X-ray spectra and ultraviolet images

The *XMM–Newton* observations used in this analysis are listed in Table 1. The data were reduced with *XMM–Newton* SAS version 6.5, and the calibration release of 2006 June. After initial processing of the EPIC MOS and pn data, spectra were extracted from a circular region of 15-arcsec radius, centred on the target. Background was obtained from a circular region of radius 150 arcsec, within which all significant sources were masked out. Appropriate response matrices and effective area files were generated with
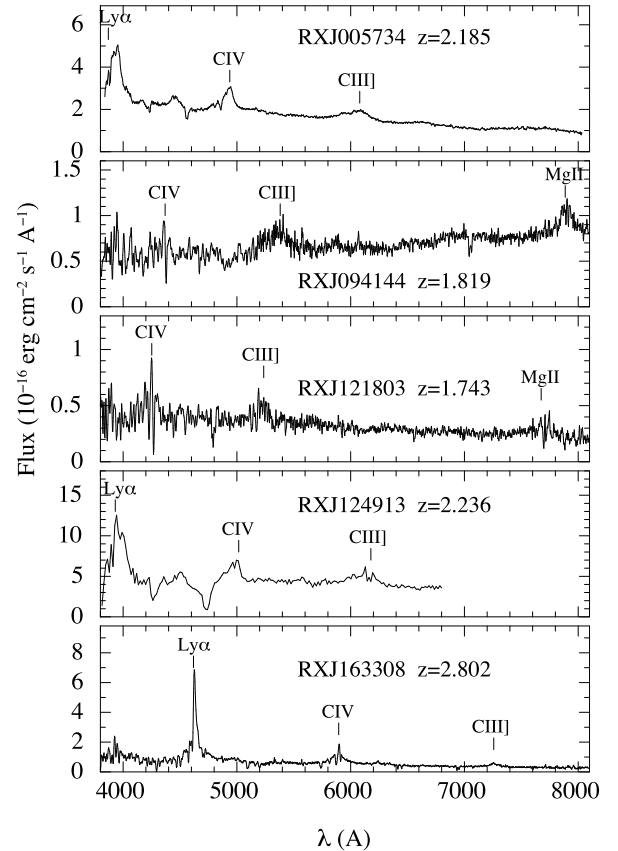


**Figure 1.** The optical spectra of RX J005734, RX J094144, RX J121803, RX J124913 and RX J163308.

the SAS tasks RMFGEN and ARFGEN. For each object, spectra and response matrices were combined using the method described in Page, Davis & Salvi (2003). To determine how the fluxes of the sources compared to those obtained in our original *ROSAT* survey, we fitted the spectra below 2 keV with a power law and fixed Galactic absorption. For RX J005734, RX J121803 and RX J163308, we obtain 0.5–2 keV fluxes of $1.2 \times 10^{-14}$, $1.5 \times 10^{-14}$ and $1.8 \times 10^{-14}$ erg cm$^{-2}$ s$^{-1}$, respectively, consistent with those obtained with *ROSAT* (Page, Mittaz & Carrera 2000). For RX J094144, we obtain a 0.5–2 keV flux of $5 \times 10^{-15}$ erg cm$^{-2}$ s$^{-1}$, approximately a quarter of its flux during our *ROSAT* survey, while for RX J124913 we obtain a 0.5–2 keV flux of $1.3 \times 10^{-14}$ erg cm$^{-2}$ s$^{-1}$, approximately half the *ROSAT* flux reported by Page et al. (2000).

Simultaneous with the X-ray observations, the *XMM–Newton* Optical Monitor (XMM-OM) took deep images in the *UVW1* filter,[1] which has an effective wavelength of 2910 Å. These observations were obtained primarily to provide photometric redshift constraints for objects surrounding the QSOs, and for the three highest redshift objects, the flux in this band is severely affected by the Lyman break. For RX J094144 and RX J121803, however, the Lyman break cuts in only at the extreme blue of the *UVW1* transmission, and will have a minor impact on the photometry. The data were reduced using the XMM-OM SAS version 6.5. The *UVW1* magnitudes of RX J094144 and RX J121803 (in the XMM-OM Vega system) are given in Table 1.

---

[1] *UVW1* images were not obtained during the July 2001 observation of RX J124913, in which the UV grism of XMM-OM was used instead.

**Table 1.** *XMM–Newton* observations. Exposure times refer to the clean exposure times after periods of high background have been excluded. The *UVW1* magnitudes for RX J094144 and RX J121803 come from the XMM-OM observations performed simultaneously with the X-ray observations, and are in the XMM-OM Vega system.

| Target | Obs ID | Date | Filters | | | Exposure time (ks) | | | *UVW1* |
|---|---|---|---|---|---|---|---|---|---|
| | | | pn | MOS1 | MOS2 | pn | MOS1 | MOS2 | (mag) |
| RX J005734.78−272827.4 | 0302310301 | 2005 December 18 | Thin | Thin | Thin | 40.2 | 47.7 | 47.3 | – |
| RX J094144.51+385434.8 | 0203270101 | 2004 May 17 | Medium | Medium | Medium | 32.6 | 40.5 | 40.8 | $21.63 \pm 0.12$ |
| RX J121803.82+470854.6 | 0203270201 | 2004 June 1 | Thin | Thin | Thin | 30.0 | 36.9 | 37.2 | $20.63 \pm 0.06$ |
| RX J124913.86−055906.2 | 0060370201 | 2001 July 11 | Thin | Thin | Thin | 25.0 | 39.6 | 39.6 | – |
| | 0203270301 | 2004 July 15 | Medium | Medium | Medium | 34.3 | 42.5 | 42.9 | – |
| RX J163308.57+570258.7 | 0302310101 | 2005 September 7 | Thin | Thin | Thin | 5.5 | 9.2 | 8.8 | – |
| | 0302310501 | 2005 October 23 | Thin | Thin | Thin | 10.5 | 19.7 | 20.0 | – |

# 3 RESULTS

## 3.1 Absorption in the rest-frame ultraviolet

Broad-band optical spectra of the five X-ray-absorbed QSOs are shown in Fig. 1. It is notable that in all five objects, at least one absorption line is superimposed on the broad C IV emission line or on the continuum to the blue of this line. To examine this more closely, we show the regions around the C IV emission line in more detail in Fig. 2. In RX J005734, there are two absorption lines apparent, with outflow velocities of 4800 and 8100 km s$^{-1}$, assuming that they are C IV. In the spectrum of RX J094144, at least one absorption line is present, apparently inflowing with a velocity of 700 km s$^{-1}$ assuming that it is C IV. As this spectrum is relatively noisy, we are unable to confirm whether the tentative absorption features to the blue of C IV are real or statistical fluctuations. There are two significant absorption features in RX J121803, one inflowing at 1200 km s$^{-1}$ and one outflowing at 1600 km s$^{-1}$. Mg II absorption is detected from the inflowing component. For RX J124913, we adopt an emission-line redshift of $z = 2.236$ (Hewitt & Burbidge 1993), although the reported emission-line redshift of this source ranges from $z = 2.22$ (Boksenberg et al. 1978) to $z = 2.244$ (Hill, Thompson & Elston 1993) depending on which emission lines the redshift is based on. Relative to this emission-line redshift, the C IV broad absorption line has a central velocity of $-16\,700$ km s$^{-1}$, with a FWHM of 5700 km s$^{-1}$ (Boksenberg et al. 1978). In RX J163308, there are four absorption lines visible, but two of these are likely to be due to an intervening absorption line system with $z = 1.482$, for which a number of other transitions are detected in the optical spectrum. The remaining two lines have outflow velocities of 800 and 7700 km s$^{-1}$. Both are accompanied by Ly$\alpha$ absorption with consistent velocities, and absorption from Si IV is detected in the 7700 km s$^{-1}$ component. The C IV absorption line properties of the five QSOs are listed in Table 2.

The five QSOs have strong rest-frame UV continuum emission. UV spectral slopes were measured from the optical spectra, longwards of Ly$\alpha$, after masking emission and absorption lines. The UV spectral slopes are listed in Table 2. With the exception of RX J094144, the UV continua of the five QSOs have spectral slopes in the range $0 < \alpha_O < 1$, which is typical for optically selected QSOs (Francis et al. 1991), indicating little or no dust reddening intrinsic to these objects. On the other hand, as can be seen in Fig. 1, the rest-frame UV continuum of RX J094144 is much redder than those of the other objects. The continuum slope in this object is $\alpha_O = 2.7$, outlying from the distribution of optically selected QSOs at the $3\sigma$ level (Francis et al. 1991), and suggesting that this object may be

somewhat dust reddened. The UV spectral shape can be matched by reddening the median Sloan Digital Sky Survey (SDSS) QSO spectrum (Vanden Berk et al. 2001) by $E(B - V) = 0.20$ using the Small Magellanic Cloud reddening law (Pei 1992), a similar level of extinction as observed in the nearby starburst/BALQSO IRAS 07598 + 6508 (Lipari 1994), and suggesting $\sim$1.4 mag of extinction at 2500 Å in the rest frame. The $UVW1 - B$ colour of RX J094144 (where the $B$ magnitude comes from Page et al. 2001b) is in reasonable agreement with this reddened template: after correction for Galactic extinction the $UVW1 - B$ colour of RX J094144 is $0.47 \pm 0.18$ compared to $UVW1 - B = 0.71$ predicted by the reddened template. In contrast, RX J121803 has a much bluer $UVW1 - B = -0.45 \pm 0.11$ after correction for Galactic extinction. For comparison, the median SDSS QSO template would have $UVW1 - B = -0.68$ at the redshift of RX J121803.

## 3.2 Modelling the X-ray spectra

Analysis of the X-ray spectra was performed using SPEX version 2.00.11.[2] As a starting point, the *XMM–Newton* spectra were fitted with a similar model to that considered by Page et al. (2001b): a power law with a fixed $\alpha_X$ of 0.98, fixed Galactic absorption and cold photoelectric absorption at the QSO redshift with $N_H$ as a free parameter. The value of $\alpha_X = 0.98$ was chosen because it is the mean spectral index of QSOs in the *XMM–Newton* energy range and at similar X-ray flux levels to our targets, as determined by Mateos et al. (2005) and confirmed in more recent work (Mateos et al. 2010). The results are given in Table 3. Although some of the individual objects are successfully fitted by this model, others are not (RX J121803 and RX J124913), and the total $\chi^2/\nu = 225/161$ for the sample of five objects is not acceptable. Therefore, we attempted to fit the spectra with two models, one in which the continuum spectral slope was allowed to vary, and one in which the ionization parameter of the absorber was allowed to vary. The spectra and model fits are shown in Fig. 3, and the confidence contours for the ionized absorber parameters are shown in Fig. 4.

As seen in Table 3, allowing the continuum spectral indices or the ionization parameters of the absorbers to vary produced acceptable values of $\chi^2/\nu$ for the five objects individually and as a sample. Since the two models are equivalent in terms of $\chi^2/\nu$, we can only discriminate between the two models by looking to see which provides the more physically plausible and self-consistent explanation for the spectra. In particular, we can test the hypothesis that the underlying spectra of these objects are reasonably typical for QSOs,

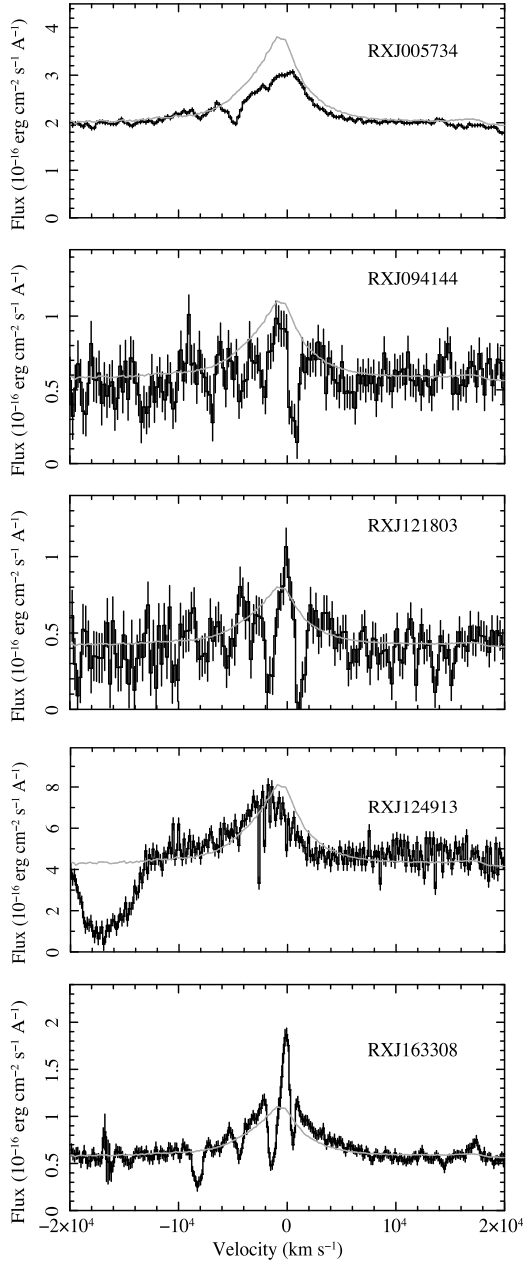---

[2] http://www.sron.nl/divisions/hea/spex/index.html

**Figure 2.** Close up of the region around the C IV 1550-Å emission line in our five X-ray-absorbed QSOs. For comparison, the grey line shows the median SDSS QSO template from Vanden Berk et al. (2001).

and their unusual observed spectral shapes are due to absorption. Two properties in particular are important in this context: the spectral index of the underlying X-ray spectrum and the ratio of optical to X-ray flux, which we parametrize as the equivalent $\alpha_{OX}$, which is the energy index of the power law that would connect the rest-frame 2500-Å and 2-keV flux densities.

Beginning with the X-ray spectral slope, the most appropriate comparison sample of normal QSOs is the sample examined by Mateos et al. (2005), which is an X-ray-selected sample with a similar flux limit to the *ROSAT* hard spectrum sample from which our targets were drawn, and measured in the same energy range, and with the same instrumentation (*XMM–Newton* EPIC) as our targets. Mateos et al. (2005) found that the distribution of QSO spectral slopes can be described as a Gaussian with a mean of $\alpha_X = 0.98$
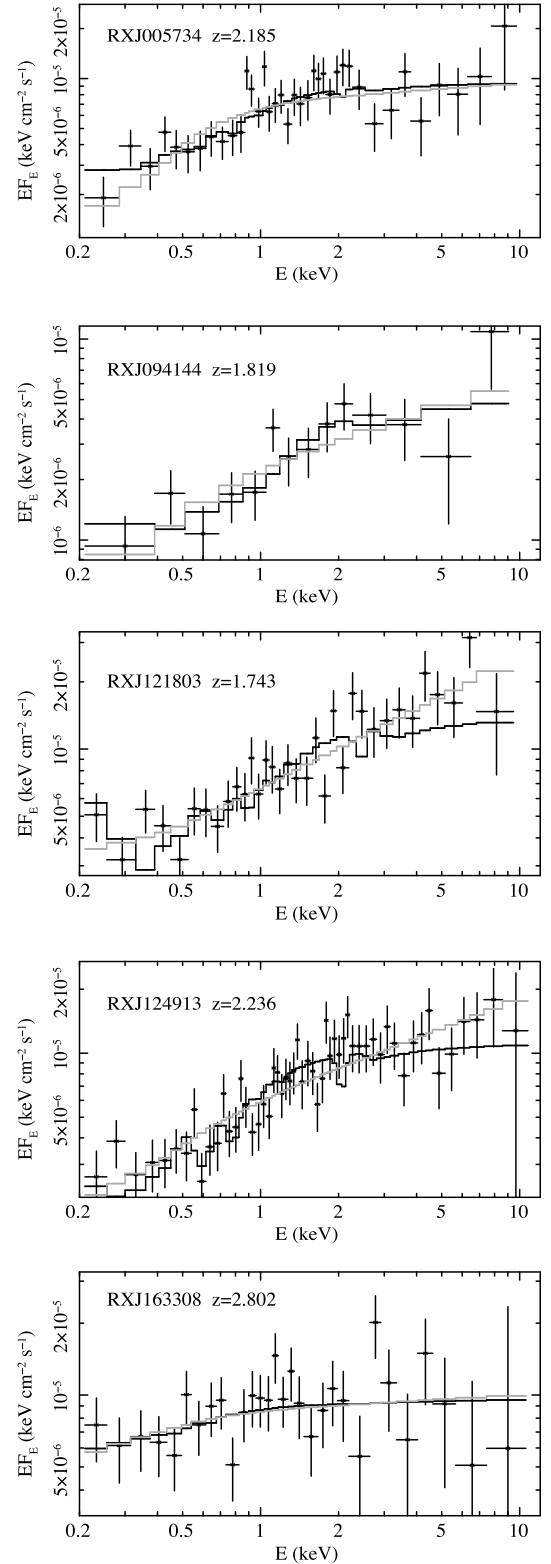


**Figure 3.** EPIC spectra of the X-ray-absorbed QSOs together with the $\alpha_X = 0.98$ power-law and ionized absorber model (black stepped line) and free-$\alpha$ power-law and cold absorber model (grey stepped line). All spectra are shown in the observer frame. Both model and data have been divided by the product of the effective area and Galactic transmission as a function of energy.
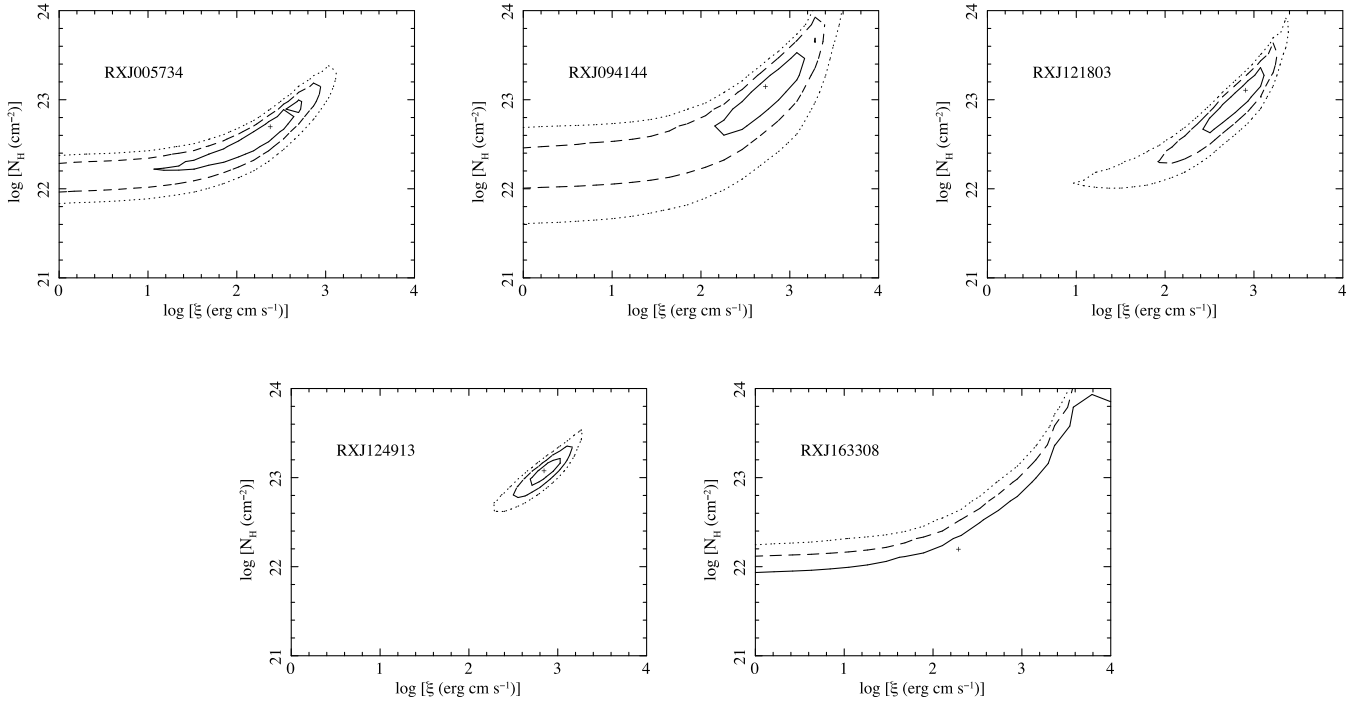
**Figure 4.** Confidence contours for $\xi$ and $N_H$ in the ionized absorber model fits to the *XMM–Newton* spectra.

**Table 2.** Characteristics of C IV UV absorption line systems and UV continuum slopes $\alpha_O$. Negative velocities correspond to blueshifted lines and positive velocities correspond to redshifted lines.

| QSO | Velocity (km s$^{-1}$) | C IV FWHM (km s$^{-1}$) | C IV EW (Å) | $\alpha_O$ |
|---|---|---|---|---|
| RX J005734 | −4800 | 500 | 5 | 0.6 |
| RX J005734 | −8100 | 500 | 2 | 0.6 |
| RX J094144 | 700 | 800 | 12 | 2.7 |
| RX J121803 | 1200 | 900 | 15 | 1.0 |
| RX J121803 | −1600 | 900 | 14 | 1.0 |
| RX J124913 | −16 700 | 5700 | 70 | 1.0 |
| RX J163308 | −800 | 700 | 11 | 0.1 |
| RX J163308 | −7700 | 700 | 10 | 0.1 |

and a standard deviation $\sigma_\alpha = 0.21$. From Table 3 we see that when the spectral slopes are allowed to vary, the best-fitting values of $\alpha_X$ for RX J005734 and RX J163308 are relatively close to the mean of the $\alpha_X$ distribution. However, the best-fitting values of $\alpha_X$ for RX J094144, RX J121803 and RX J124913 are all unusually low, lying within the lowest 3 per cent of the distribution. This is an unlikely circumstance if the intrinsic photon indices of our sample were drawn from the same distribution as QSOs in general, and suggests that the cold photoelectric absorption does not fully account for the unusual X-ray spectral shapes observed in these objects. In comparison, the spectral slopes are fixed in the ionized absorber model, and so are by design consistent with a typical underlying QSO spectrum.

Moving to $\alpha_{OX}$, we have calculated this quantity for each of the model fits and each of the QSOs. In each case, the rest-frame 2500-Å flux has been estimated from the B magnitude listed in Page et al. (2001b), assuming an optical slope of $\alpha_O = 0.5$. The 2-keV flux is

determined from the continuum model of the X-ray spectral fit, i.e. it is the intrinsic continuum flux, corrected for the modelled X-ray absorption.

The distribution of $\alpha_{OX}$ in normal QSOs is known to depend on luminosity (Vignali, Brandt & Schneider 2003; Strateva et al. 2005), and there is inevitably a selection bias depending on whether the sample is X-ray or optically selected. The most appropriate reference distribution of $\alpha_{OX}$ in the literature is that presented in Strateva et al. (2005) for a sample of 155 SDSS QSOs with medium-deep *ROSAT* coverage. However, since this distribution is based on an optically selected sample, while our sample is X-ray selected, we have constructed a reference distribution of $\alpha_{OX}$ for X-ray-selected QSOs drawn from the *ROSAT* International X-ray Optical Survey (RIXOS; Mason et al. 2000). We restrict the reference sample to those RIXOS QSOs at $z > 1$, which corresponds to a similar luminosity range to our X-ray-absorbed QSO sample, because RIXOS has a similar X-ray flux limit to the *ROSAT* hard spectrum survey from which our targets were drawn. We calculated $\alpha_{OX}$ for the reference sample in an identical fashion to our absorbed QSO sample except that we assume no intrinsic X-ray absorption and $\alpha_X = 0.98$ for the RIXOS AGN. The reference sample has a mean $\langle\alpha_{OX}\rangle = 1.49$ and a standard deviation $\sigma_{OX} = 0.16$; the distribution of $\alpha_{OX}$ for the reference sample is shown in Fig. 5. For comparison, the SDSS sample presented in Strateva et al. (2005) has a very similar distribution of $\alpha_{OX}$, with $\langle\alpha_{OX}\rangle = 1.48$ and $\sigma_{OX} = 0.18$.

In Table 3 we see that with the exception of RX J124913, the absorbed QSOs have $\alpha_{OX}$ values within two standard deviations of $\langle\alpha_{OX}\rangle$ for the reference distribution. For RX J124913, the level of discrepancy depends strongly on the X-ray spectral model. The ionized absorber fit gives the most consistent $\alpha_{OX}$ value, at 2.3 standard deviations from the mean of the reference sample, while the fit with a cold absorber and fitted $\alpha_X$ gives the most discrepant value of $\alpha_{OX} = 1.96$, >2.9 standard deviations from the mean of the reference sample. Indeed, this value of $\alpha_{OX}$ is larger than any $\alpha_{OX}$ in the RIXOS reference sample or the SDSS sample of Strateva

**Table 3.** Model fits to the *XMM–Newton* spectra. The models are a combination of a power law (PL), and either a cold photoelectric absorber (CA) or warm, ionized absorber (WA) at the redshift of the AGN. In addition, a zero-redshift cold absorber with column density fixed at the Galactic value is included in each model. Parameters marked 'f' are fixed in the fit, and '*' is used to indicate an uncertainty in a model parameter that is not constrained by the fit. $N_H$ has units of cm$^{-2}$ and $\xi$ has units of erg cm s$^{-1}$.

| | RX J005734 | RX J094144 | RX J121803 | RX J124913 | RX J163308 | Total |
|---|---|---|---|---|---|---|
| PL×CA | | | | | | |
| $\alpha_X$ | 0.98$^f$ | 0.98$^f$ | 0.98$^f$ | 0.98$^f$ | 0.98$^f$ | |
| $\log N_H$ | $22.0^{+0.1}_{-0.1}$ | $22.1^{+0.2}_{-0.2}$ | $21.8^{+0.1}_{-0.1}$ | $22.2^{+0.1}_{-0.1}$ | $21.5^{+0.2}_{-0.4}$ | |
| $\alpha_{OX}$ | $1.70^{+0.05}_{-0.06}$ | $1.48^{+0.30}_{-0.12}$ | $1.32^{+0.06}_{-0.05}$ | $1.89^{+0.09}_{-0.09}$ | $1.44^{+0.05}_{-0.04}$ | |
| $\chi^2/\nu$ | 41/36 | 15/12 | 64/32 | 82/53 | 22/28 | 225/161 |
| PL×CA | | | | | | |
| $\alpha_X$ | $0.82^{+0.10}_{-0.09}$ | $0.57^{+0.19}_{-0.17}$ | $0.41^{+0.07}_{-0.06}$ | $0.53^{+0.07}_{-0.07}$ | $0.94^{+0.15}_{-0.13}$ | |
| $\log N_H$ | $21.8^{+0.2}_{-0.2}$ | $21.5^{+0.4}_{-0.9}$ | $0.00^{+21.9}_{-*}$ | $21.5^{+0.2}_{-0.3}$ | $21.4^{+0.4}_{-*}$ | |
| $\alpha_{OX}$ | $1.71^{+0.05}_{-0.06}$ | $1.54^{+0.52}_{-0.13}$ | $1.39^{+0.07}_{-0.06}$ | $1.96^{+0.10}_{-0.10}$ | $1.43^{+0.05}_{-0.04}$ | |
| $\chi^2/\nu$ | 39/35 | 11/11 | 29/31 | 50/52 | 22/27 | 151/156 |
| PL×WA | | | | | | |
| $\alpha_X$ | 0.98$^f$ | 0.98$^f$ | 0.98$^f$ | 0.98$^f$ | 0.98$^f$ | |
| $\log \xi$ | $2.4^{+0.2}_{-0.3}$ | $2.7^{+0.4}_{-0.4}$ | $2.9^{+0.2}_{-0.4}$ | $2.9^{+0.1}_{-0.1}$ | $2.3^{+1.0}_{-6.3*}$ | |
| $\log N_H$ | $22.7^{+0.2}_{-0.2}$ | $23.2^{+0.4}_{-0.4}$ | $23.1^{+0.3}_{-0.3}$ | $23.1^{+0.1}_{-0.1}$ | $22.2^{+1.0}_{-0.7}$ | |
| $\alpha_{OX}$ | $1.68^{+0.05}_{-0.06}$ | $1.43^{+0.17}_{-0.10}$ | $1.26^{+0.04}_{-0.04}$ | $1.85^{+0.08}_{-0.08}$ | $1.43^{+0.05}_{-0.04}$ | |
| $\chi^2/\nu$ | 34/35 | 9/11 | 43/31 | 51/52 | 21/27 | 158/156 |
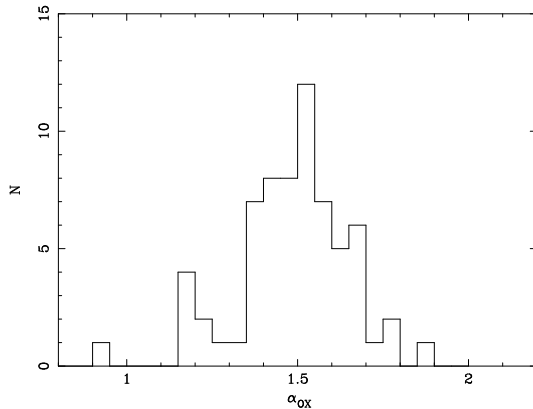


**Figure 5.** Reference $\alpha_{OX}$ distribution for $z > 1$ RIXOS X-ray-selected QSOs, as described in Section 3.2.

et al. (2005), suggesting that the model with a cold absorber and the continuum slope fitted as a free parameter would also require a highly unusual spectral energy distribution (SED) for RX J124913. While RX J094144 has rather typical values of $\alpha_{OX}$ in Table 3, we note that if we correct for the intrinsic extinction equivalent to $E(B - V) = 0.2$, suggested by the UV continuum shape (Section 3.1), then the $\alpha_{OX}$ would increase by 0.40, leading to an abnormal $\alpha_{OX}$ for the cold absorber, fitted $\alpha_X$ model for this source as well as for RX J124913.

Overall, the ionized absorber model is consistent with the five QSOs having unremarkable underlying X-ray continua and optical to X-ray SEDs. In contrast, if the X-ray absorbers are modelled as cold gas, the QSOs require a combination of cold absorption, unusual X-ray continua and unusual optical to X-ray SEDs. We therefore consider that the ionized absorber model provides a simpler, less contrived solution than the model in which the X-ray absorber is cold. We also note that the presence of C IV absorption lines with equivalent width (EW) >5 Å in the rest-frame UV spec-

tra of all five QSOs (and Si IV in RX J124913 and RX J163308) provides independent confirmation that these objects are viewed through columns of ionized gas. Therefore, in what follows we adopt the ionized absorber fits as the best description of the X-ray spectra.

## 4 DISCUSSION

### 4.1 Characteristics of the absorbers

Our study has revealed absorption from ionized gas in both the rest-frame UV spectra and in the X-ray spectra of our sample of X-ray-absorbed QSOs. In the nearby Universe, ionized absorbers are common in Seyfert galaxies (e.g. Reynolds 1997; George et al. 1998), and have been studied in some detail (Steenbrugge et al. 2005; Blustin et al. 2007). Therefore, in trying to understand the properties of our sample of X-ray-absorbed QSOs, it is instructive to compare them with those found in Seyfert galaxies. Amongst Seyfert galaxies, ionized absorption is observed primarily in broad-line (type 1) objects (e.g. Reynolds 1997; George et al. 1998; Blustin et al. 2005), indicating that the ionized absorbers lie within the ionization cones of the AGN, assuming the standard AGN geometric unification scheme in which the central regions are surrounded by a dusty, obscuring torus (Antonucci 1993). The presence of ionized absorption within our X-ray-absorbed QSOs is therefore in keeping with a normal pole-on orientation for these objects.

The ionized column densities, and the degree of soft X-ray attenuation, of our X-ray-absorbed QSOs are considerably higher than are found in the majority of nearby Seyferts: with the exception of RX J163308 for which the X-ray absorber properties are poorly constrained, all of our sample have best-fitting $\log N_H > 22.5$, whereas only three of the 23 AGN in the sample studied by Blustin et al. (2005) have $\log N_H > 22.5$. None the less, a few nearby objects such as NGC 3783 do have comparable column densities and ionization states (Blustin et al. 2002; Krongold et al. 2003; Netzer et al. 2003;

Reeves et al. 2004). The ionized absorbers in Seyferts typically contain ions covering a large range of ionization, and where good data are available they almost always require multiple phases with different ionization parameters to model their spectra (Blustin et al. 2005; McKernan, Yaqoob & Reynolds 2007). Moving to higher luminosity objects, ionized absorbers appear to be common in QSOs, with the studies of Porquet et al. (2004) and Piconcelli et al. (2005) suggesting that around 50 per cent of low-redshift QSOs show some evidence for ionized absorption in their X-ray spectra. However, column densities of ionized material similar to those found in our sample of X-ray-absorbed QSOs are relatively rare, with Piconcelli et al. (2005) finding that only two of their sample of 40 nearby QSOs have ionized absorbers with best-fitting $\log N_H > 22.5$. In the small number of nearby QSOs which have well-characterized ionized absorbers with $N_H > 10^{22}\,\mathrm{cm}^{-2}$, notably PG 1114+445 (Ashton et al. 2004), PDS 456 (Reeves, O'Brien & Ward 2003), H 0557 − 385 (Ashton et al. 2006) and PG 1211+143 (Pounds et al. 2003), the absorbers are found to have multiple ionization phases, in common with the well-studied Seyfert warm absorbers.

On this basis, we can expect that the parameters determined for the single phase absorbers in our sources are therefore likely to be representative only of the dominant phase of absorption, and the high-$\xi$ absorption which we have detected is likely to be accompanied by significant soft X-ray absorption due to material with $\log \xi < 1.5$. In fact the multi-ionization-phase nature of the ionized absorbers is implied by the absorption lines detected in their UV spectra. The best-fitting ionized X-ray absorber models for all five objects produce insignificant C IV absorption lines (EW < 1 Å), in contrast to the large EW lines (>5 Å) that are measured in their rest-frame UV spectra, implying that at least two ionization phases of absorber are required to produce both UV and X-ray absorption. Note that while absorption from C IV is seen in about half of QSOs (Vestergaard 2003), C IV absorption lines with EW >5 Å are relatively rare. Only three out of 114 non-BALQSOs studied by Vestergaard (2003) show C IV absorption with such large EW. Combined with the statistic that ∼15 per cent of QSOs have C IV BALs, which by definition have C IV EW > 5 Å (Tolea, Krolik & Tsvetanov 2002; Gibson et al. 2009), we can conservatively estimate the incidence of C IV absorption lines with EW > 5 Å to be 20 per cent. The probability of all five of our X-ray-absorbed QSOs having such absorption lines if they were drawn randomly from the population is therefore $0.2^5 = 3 \times 10^{-4}$, and hence the connection of the C IV absorbers with the X-ray absorption is quite secure.

Our finding that the X-ray absorbers in our sample are highly ionized allows us to address the puzzling absence of strong UV attenuation by dust, despite the large column densities of X-ray-absorbing gas. Nearby Seyfert 1 galaxies with warm absorbers also show this property: the column densities of X-ray-absorbing gas can be large, but they have bright UV continua with broad emission lines, e.g. NGC 3783 has $\log N_H > 22.5$ (Netzer et al. 2003; Reeves et al. 2004) as well as a strong UV continuum and broad UV emission lines with little reddening (Crenshaw & Kraemer 2001; Evans & Koratkar 2004).

As a corollary to the apparent similarity between the ionized absorbers found in our X-ray-absorbed QSOs and some nearby Seyferts, we might wonder whether star formation is associated with such X-ray absorption in objects such as NGC 3783, as it is in X-ray-absorbed QSOs. A systematic investigation of this issue is beyond the scope of this paper, but it is interesting to note that NGC 3783 has a 2–10 keV X-ray luminosity of $1.3 \times 10^{43}\,\mathrm{erg\,s}^{-1}$ and an infrared (IR) luminosity of $3 \times 10^{10}\,\mathrm{L}_\odot$ (Mullaney et al. 2011), so that if we scaled its SED to match the X-ray luminosities of

our X-ray-absorbed QSOs its IR luminosity would be in the regime of ultraluminous IR galaxies, commensurate with a substantial star formation rate.

## 4.2 Comparison to soft X-ray-weak QSOs

It is interesting to compare the X-ray-absorbed QSOs with another population of unusual QSOs: those that are classified as soft X-ray weak. These objects are characterized by large values of $\alpha_{OX}$, and represent around 10 per cent of optically selected QSOs (Laor et al. 1997). Brandt, Laor & Wills (2000) found a strong correlation between $\alpha_{OX}$ and the EW of C IV absorption, which is found to be >4 Å in the majority of soft X-ray-weak QSOs. This was interpreted by Brandt et al. (2000) as evidence that soft X-ray-weak QSOs are such because they are absorbed in the soft X-ray band. As shown in Section 3.1, the QSOs in our sample all have C IV absorption lines with EW > 4 Å, similar to the C IV lines found in soft X-ray-weak QSOs. More recently, *XMM–Newton* observations of soft X-ray-weak QSOs have indicated that this absorption is primarily due to ionized gas (Brinkmann, Papadakis & Ferrero 2004; Piconcelli, Jiménez-Bailón & Guainazzi 2004; Schartel et al. 2005), with ionization parameters ranging from $\log \xi = 1.9$ to 3.2 and column densities ranging from $3 \times 10^{22}$ to $2 \times 10^{23}\,\mathrm{cm}^{-2}$. These column densities and ionization parameters are remarkably similar to those of our X-ray-absorbed QSOs. Given these similarities, we might expect that intense star formation would be as common in soft X-ray-weak QSOs as it is in X-ray-absorbed QSOs. To our knowledge, there has been no systematic study of the star formation rates in soft X-ray-weak QSOs, but there are certainly well-known examples of soft X-ray-weak QSOs which are rapidly forming stars, notably Mrk 231 and IRAS 07598 + 6508 (Lipari 1994).

## 4.3 Location of the absorbers

We now consider the location, physical nature and implications of the ionized absorbers found in our sample. To estimate the location, we assume that the absorber is in the form of an outflowing wind originating at a distance $R_{abs}$ from the continuum source with density $n \propto r^{-2}$. From the definition of the ionization parameter,

$$\xi = L_{ion}/(nr^2), \tag{1}$$

where $L_{ion}$ is the 1–1000 Rydberg ionizing luminosity in $\mathrm{erg\,s}^{-1}$, such a wind will have an ionization parameter $\xi$ that is constant with radius $r$. To take account that the winds from AGN are likely to be clumpy or filamentary, we characterize the outflow with a macroscopic volume-filling factor $f < 1$. The column density of the absorber is dominated by material close to the base of the outflow, and hence $R_{abs}$ can be taken as the characteristic distance of the absorber from the continuum source. Integrating the density along the line of sight, we obtain $N_H = fR_{abs}n_{abs}$, where $n_{abs}$ is the density at the base of the outflow. Substituting $n_{abs}$ for $n$ in equation (1), we obtain the relation

$$R_{abs} = \frac{L_{ion}f}{\xi N_H}. \tag{2}$$

To estimate $L_{ion}$ we assume that below 0.35 keV, the SED has the functional form given by Mathews & Ferland (1987) for a QSO ionizing spectrum, in which the X-ray power law steepens to $\alpha = 3$ in the range 56–350 eV, and has a slope of $\alpha = 1.0$ in the 24–56 eV range, below which it has a slope of $\alpha_O = 0.5$. This SED of Mathews & Ferland (1987) was constructed to be appropriate for objects of QSO luminosity, and when joined to our $\alpha_X = 0.98$ spectrum at 0.35 keV it has $\alpha_{OX} = 1.47$.

**Table 4.** Characteristic scales and outflow rates for the sample of X-ray-absorbed QSOs. $L_{ion}$ is the 1–1000 Rydberg ionizing luminosity in erg s$^{-1}$, $R_{abs}$ is the distance of the base of the absorber from the continuum source in cm, $R_{torus}$ is the distance of the inner edge of the dusty torus from the continuum source in cm, $\dot{M}_{acc}$ is the mass accretion rate and $\dot{M}_{out}$ is the mass outflow rate in the ionized absorber. An '∗' indicates a confidence limit that is not constrained by the data. Note that the uncertainties are purely statistical and do not include the systematic uncertainty on the filling factor, $f$, on which both $R_{abs}$ and $\dot{M}_{out}$ depend linearly. As explained in Section 4.3, we estimate an uncertainty on $\log f$ of ~0.8.

| Object | $\log L_{ion}$ | $\log R_{abs}$ | $\log R_{torus}$ | $\log(\dot{M}_{out}/\dot{M}_{acc})$ |
|---|---|---|---|---|
| RX J005734 | 46.7 | $19.6^{+0.7}_{-0.4}$ | 19.4 | $1.1^{+0.4}_{-0.3}$ |
| RX J094144 | 46.2 | $18.4^{+0.6}_{-0.8}$ | 19.2 | — |
| RX J121803 | 46.6 | $18.6^{+0.5}_{-0.6}$ | 19.4 | $-0.1^{+0.4}_{-0.2}$ |
| RX J124913 | 46.8 | $18.8^{+0.3}_{-0.2}$ | 19.5 | $0.9^{+0.2}_{-0.1}$ |
| RX J163308 | 47.0 | $20.7^{+*}_{-2.4}$ | 19.5 | $1.2^{+*}_{-1.2}$ |

For the fixed $\alpha_X = 0.98$, which we have taken in our ionized absorber model fits, $L_{ion}$ is a factor of 44.3 times larger than the rest-frame 2–10 keV luminosity. For the filling factor, $f$, we assume a value of $\log f = -2$, which is the average $\log f$ for ionized absorbers with $\xi > 0.7$ in Seyfert galaxies found by Ashton et al. (2006). The derived values of $L_{ion}$ and $R_{abs}$ are given in Table 4. With the exception of RX J163308, for which $R_{abs}$ is very poorly constrained, the best-fitting values of $R_{abs}$ range from 1 to 15 pc. The uncertainties given for $R_{abs}$ are derived from the statistical uncertainties on the product $\xi \times N_H$, and so do not include the uncertainty on the volume-filling factor. As an estimate of this additional uncertainty, we note that Ashton et al. (2006) obtained a standard deviation in $\log f$ of 0.8 for Seyfert warm absorbers with $\xi > 0.7$. For comparison, we also provide in Table 4 the locations of the inner edge of the dusty torus $R_{torus}$ for our sources, calculated using equation (5) from Barvainis (1987), with a dust sublimation temperature of 1260 K (as implied by the composite near-IR QSO spectrum obtained by Glikman, Helfand & White 2006) and taking the UV luminosity to be equal to $L_{ion}$. We see that $R_{abs}$ is in all cases smaller than, or consistent with, $R_{torus}$.

It would therefore be natural to assume that the absorbers originate in the AGN themselves, rather than in their host galaxies. This solution is attractive, because it is compatible with the lack of optical extinction in these objects: if the absorber is driven as a wind, either from the accretion disc or from evaporation of the inner edge of the molecular torus, then dust will be sublimated before (or as) it enters the flow. With this in mind, it is instructive to obtain upper limits for the distance of the absorbing gas from the nucleus at which it could remain ionized by the AGN radiation field, using equation (2) and taking the limit case of filling factor $f = 1$. Doing so, we find that the X-ray absorbers in RX J094144, RX J121803 and RX J124913 must lie within a few hundred parsecs of the ionizing source, within or close to the AGN rather than being distributed throughout the host galaxy.

A key indicator of the importance of an ionized AGN wind is the ratio of the mass outflow rate $\dot{M}_{out}$ to the accretion rate $\dot{M}_{acc}$. To determine this ratio, we first take $L_{ion}$ to be $0.6 \times L_{acc}$ (Vasudevan & Fabian 2009), where $L_{acc}$ is the bolometric accretion luminosity, so that

$$L_{ion} = 0.6 L_{acc} = 0.6 \epsilon \dot{M}_{acc} c^2, \tag{3}$$

where $c$ is the speed of light and $\epsilon$ is the accretion efficiency. We can obtain the mass outflow rate of the wind using equation (18)

from Blustin et al. (2005):

$$\dot{M}_{out} = \frac{1.23 m_p L_{ion} f v \Omega}{\xi}, \tag{4}$$

where $m_p$ is the rest mass of a proton, $v$ is the outflow velocity and $\Omega$ is the solid angle of the outflow. Combining equations (3) and (4), we obtain

$$\dot{M}_{out}/\dot{M}_{acc} = 0.74 m_p f v \Omega \epsilon c^2/\xi. \tag{5}$$

We take $\epsilon = 0.1$, and as before we assume $f = 0.01$. We take the opening angle of the outflow $\Omega = \pi$ sr, corresponding to the opening angle of the torus inferred from the type 1/type 2 number ratio in nearby Seyferts (Maiolino & Rieke 1995). For the velocity $v$ we assume that the X-ray-absorbing ionized outflow is associated with the fastest outflow identified in the rest-frame UV (Table 2). This is a reasonable estimate, since the highest ionization absorbers are typically (though not always) the highest velocity systems in individual Seyfert galaxies (e.g. Sako et al. 2003; Steenbrugge et al. 2005; Costantini et al. 2007). At the same time, it is a conservative estimate (i.e. may underestimate the mass outflow rate) for two reasons: first, the signal-to-noise ratios of our optical spectra (particularly for RX J094144 and RX J121803) are not high enough that we can be confident we have identified all of the absorption line systems, and secondly, our estimates of the systemic velocities are based on the UV broad emission lines, which themselves are frequently observed to have a net outflow velocity of the order of 1000 km s$^{-1}$ (Espey et al. 1989). The derived values of $\log \dot{M}_{out}/\dot{M}_{acc}$ are listed in Table 4. In the case of RX J094144, the C IV absorption line that is identified in the rest-frame UV spectrum is redshifted with respect to the UV emission lines, so its true velocity with respect to the system is too uncertain for us to attempt to estimate the mass outflow rate. The mass outflow rates derived for RX J005734, RX J124913 and RX J163308 are about 10 times their mass accretion rates, while in RX J121803 the accretion and outflow rates are comparable.

### 4.4 Implications for QSO evolution

At this point, it is worth considering how these results bear on the broader picture of how X-ray-absorbed QSOs relate to the evolution of massive black holes and their host galaxies. In Page et al. (2004), we argued that the submillimetre properties of X-ray-absorbed QSOs imply an evolutionary sequence in which SMGs evolve into QSOs, with the X-ray-absorbed QSOs representing a brief, transitional phase between these two stages. The discovery that SMGs typically contain more heavily absorbed, lower luminosity AGN than X-ray-absorbed QSOs supports this evolutionary picture (Alexander et al. 2005). In Stevens et al. (2005), we further proposed that the X-ray-absorbed QSOs are in the process of driving the interstellar media out of their host galaxies via radiatively driven winds, in accord with the models developed by Silk & Rees (1998), Fabian (1999), Granato et al. (2004) and Di Matteo, Springel & Hernquist (2005). Now, with our *XMM–Newton* observations we have shown that the X-ray absorption in these objects is indeed due to substantial, ionized, QSO-driven winds. The space density of X-ray-absorbed QSOs is ~15 per cent that of unabsorbed QSOs (Page et al. 2004; Silverman et al. 2005; Page et al. 2006), implying that if all QSOs go through an X-ray-absorbed phase in their evolution, this phase lasts only ~15 per cent as long as the unabsorbed phase. These relative lifetimes may be a natural consequence of the high mass outflow rates in the X-ray-absorbed QSOs: for the majority of our X-ray-absorbed QSOs, we estimate a mass outflow rate

which is ∼10 times higher than the accretion rate, implying that the fuel supply will be depleted 10 times faster in an X-ray-absorbed QSO than in an unabsorbed QSO for the same accretion rate and fuel reservoir. However, this argument is more complicated if the two types of QSOs fit within the evolutionary sequence discussed above, because in this case the fuel supply for an unabsorbed QSO will consist only of the fuel that remains after the X-ray-absorbed phase. None the less, if material is ejected at ∼10 times the accretion rate for ∼15 per cent of the (X-ray-absorbed + unabsorbed) QSO lifetime, the total mass of material ejected by the QSO will be of the same order as that accreted.

The origin of the ionized, absorbing gas is then a fundamental issue for the physics of X-ray-absorbed QSOs and their evolution. Assuming that X-ray-absorbed QSOs have the usual AGN structure envisaged in geometric unification schemes, the two obvious sources of material are the accretion disc and the dusty torus. If the wind is driven from the accretion disc, the ejected material must pass through the accretion disc during the X-ray-absorbed phase; in this case, it is difficult to understand why this happens on a time-scale which is short compared to the lifetime of the QSO. On the other hand, if the ionized wind is driven from the torus, then the time-scale for the X-ray-absorbed phase corresponds to the time required to erode the inner part of the torus and so enlarge substantially its opening angle; as shown by Krolik & Kriss (2001) this time-scale can be much shorter than the lifetime of the QSO. For accretion at the Eddington rate, the escape velocities at the distances of the inner edge of the torus (as given in Table 4) are between 900 and 1500 km s$^{-1}$, and scale inversely with the square root of the accretion rate in Eddington units. Hence, of our X-ray-absorbed QSOs, only the BALQSO RX J124913 has outflow velocities which are too high to plausibly be associated with an outflow from the inner edge of the torus, implying an accretion disc origin for its outflow.

Viable AGN feedback models which reproduce the $M-\sigma$ relation generally incorporate the feedback in the form of kinetic energy given to gas within the immediate (∼100 pc) environment of the AGN (e.g. Fabian 1999; Granato et al. 2004; Di Matteo et al. 2005; Hopkins et al. 2006; Sijacki et al. 2007), which then interacts with gas on a larger scale to terminate star formation in the host spheroid. It is generally agreed that of the order of 5 per cent of the AGN radiative output must be fed back as kinetic energy in order for the models to succeed (Silk & Rees 1998; Wyithe & Loeb 2003; Di Matteo et al. 2005). We can make a simple estimate for the kinetic energy of the outflows compared to the radiative output of the X-ray-absorbed QSOs as follows. We take the total energy radiated during the X-ray-absorbed phase to be $E_T = \epsilon M_{acc} c^2$, where $\epsilon$ is the radiative efficiency, $c$ is the speed of light and $M_{acc}$ is the mass accreted during the X-ray-absorbed phase. The kinetic energy built up by the outflow is $E_O = 0.5 M_{out} v^2$, where $M_{out}$ is the mass supplied to the outflow during the X-ray-absorbed phase and $v$ is the velocity of the outflow. The fraction of the radiated output of the QSO which is fed back to the surrounding gas as kinetic energy of the outflow is then

$$\frac{E_O}{E_T} = \frac{0.5}{\epsilon} \times \frac{M_{out}}{M_{acc}} \times \frac{v^2}{c^2}. \qquad (6)$$

If we take $M_{out}/M_{acc} = \dot{M}_{out}/\dot{M}_{acc} \sim 10$ for the X-ray-absorbed phase (as we find for the majority of our X-ray-absorbed QSOs), and a typical outflow velocity of 8000 km s$^{-1}$ (see Table 2), then we obtain $E_O/E_T \sim 4$ per cent. The value of $E_O/E_T$ so derived is independent of the radiative efficiency $\epsilon$, because the $\epsilon$ in equation (6) cancels with that in equation (5) from which $\dot{M}_{out}/\dot{M}_{acc}$ is obtained. On the other hand, the uncertainty on $\dot{M}_{out}/\dot{M}_{acc}$ is in truth very large

(> a factor of 10), depending on the unknown filling factor, $f$, and the square of the outflow velocity, $v$, which may not be the same for the X-ray-absorbing phase as the UV absorber. None the less, $E_O/E_T \sim 4$ per cent is quite consistent with the level of feedback required to terminate star formation and produce the $M-\sigma$ relation, implying that the ionized outflows in X-ray-absorbed QSOs could plausibly be the mechanism through which star formation is terminated in massive galaxies.

## 5  CONCLUSIONS

We have presented X-ray spectra from *XMM–Newton* EPIC and rest-frame UV spectra from ground-based telescopes for five X-ray-absorbed, submillimetre-luminous QSOs. All five QSOs exhibit strong C IV absorption lines in their UV spectra with EW >5 Å. The X-ray spectra can be modelled successfully in terms of $\chi^2$ with either cold or ionized absorbers. The cold X-ray absorber model requires that the QSOs have unusually flat X-ray continuum shapes and unusual optical to X-ray SEDs, while the ionized absorber model does not require abnormal underlying continuum properties. This finding, coupled with the presence of strong C IV absorption lines in the UV, leads us to favour the ionized absorber model over the cold absorber model. Assuming that the X-ray absorbing gas is outflowing with the same velocities as the C IV absorbers, we are able to investigate the likely location, mass outflow rates and energetics of the ionized absorbers. We find that the X-ray-absorbing gas is likely to be located within 10 pc of the continuum source, and so is associated with the active nucleus rather than the surrounding host galaxy's interstellar medium. We estimate that the fraction of radiated power that is converted into kinetic luminosity of the outflowing winds is typically ∼4 per cent, in agreement with estimates for the kinetic feedback from QSOs that is required to produce the $M-\sigma$ relation. This finding is thus consistent with the hypothesis that X-ray-absorbed QSOs represent the transition phase between obscured accretion and the luminous QSO phase in the evolution of massive galaxies.

## REFERENCES

Alexander D. M., Smail I., Bauer F. E., Chapman S. C., Blain A W., Brandt
    W. N., Ivison R. J., 2005, Nat, 433, 604
Almaini O. et al., 2003, MNRAS, 338, 303
Antonucci R., 1993, ARA&A, 31, 473
Ashton C. E. et al., 2004, MNRAS, 355, 73

Ashton C. E., Page M. J., Branduardi-Raymont G., Blustin A. J., 2006, MNRAS, 366, 521

Barvainis R., 1987, ApJ, 320, 537

Blustin A. J., Branduardi-Raymont G., Behar E., Kaastra J. S., Kahn S. M., Page M. J., Sako M., Steenbrugge K. C., 2002, A&A, 392, 453

Blustin A. J., Page M. J., Fuerst S. V., Branduardi-Raymont G., Ashton C. E., 2005, A&A, 431, 111

Blustin A. J. et al., 2007, A&A, 466, 107

Boksenberg A., Carswell R. F., Smith M. G., Whelan J. A. J., 1978, MNRAS, 184, 773

Brandt W. N., Laor A., Wills B. J., 2000, ApJ, 528, 637

Brinkmann W., Papadakis I., Ferrero E., 2004, A&A, 414, 107

Coppin K. E. K. et al., 2008, MNRAS, 389, 45

Costantini E. et al., 2007, A&A, 461, 121

Crenshaw D. M., Kraemer S. B., 2001, ApJ, 562, L29

Di Matteo T., Springel V., Hernquist L., 2005, Nat, 433, 604

Espey B. R., Carswell R. F., Bailey J. A., Smith M. G., Ward M. J., 1989, ApJ, 342, 666

Evans I. N., Koratkar A. P., 2004, ApJS, 150, 73

Fabian A. C., 1999, MNRAS, 308, L39

Fabian A. C. et al., 2000, MNRAS, 315, L8

Francis P. J., Hewett P. C., Foltz C. B., Chaffee F. H., Weymann R. J., Morris S. L., 1991, ApJ, 373, 465

George I. M., Turner T. J., Netzer H., Nandra K., Mushotzky R. F., Yaqoob T., 1998, ApJS, 114, 73

Gibson R. R. et al., 2009, ApJ, 692, 758

Glikman E., Helfand D. J., White R. L., 2006, ApJ, 640, 579

Granato G. L., De Zotti G., Silva L., Bressan A., Danese L., 2004, ApJ, 600, 580

Hewitt A., Burbidge G., 1993, ApJS, 87, 451

Hill G. J., Thompson K. L., Elston R., 1993, ApJ, 414, L1

Hopkins P. F., Hernquist L., Cox T. J., Di Matteo T., Robertson B., Springel V., 2006, ApJS, 163, 1

Hughes D. H. et al., 1998, Nat, 394, 241

Junkkarinen V. T., Burbidge E. M., Smith H. E., 1987, ApJ, 317, 460

Krolik J. H., Kriss G. A., 2001, ApJ, 561, 684

Krongold Y., Nicastro F., Brickhouse N. S., Elvis M., Liedahl D., Mathur S., 2003, ApJ, 597, 832

Laor A., Fiore A., Elvis M., Wilkes B. J., McDowell J. C., 1997, ApJ, 477, 93

Lipari S., 1994, ApJ, 436, 102

Lutz D. et al., 2010, ApJ, 712, 1287

McKernan B., Yaqoob T., Reynolds C. S., 2007, MNRAS, 379, 1359

McMahon R. G., Priddey R. S., Omont A., Snellen I., Withington S., 1999, MNRAS, 309, L1

Magorrian J. et al., 1998, AJ, 115, 2285

Maiolino R., Rieke G. H., 1995, ApJ, 454, 95

Mason K. O. et al., 2000, MNRAS, 311, 456

Mateos S. et al., 2005, A&A, 433, 855

Mateos S. et al., 2010, A&A, 510, 35

Mathews W. G., Ferland G. J., 1987, ApJ, 323, 456

Merritt D., Ferrarese L., 2001, MNRAS, 320, L30

Mullaney J. R., Alexander D. M., Goulding A. D., Hickox R. C., 2011, MNRAS, 414, 1082

Netzer H. et al., 2003, ApJ, 599, 933

Page M. J., Mittaz J. P. D., Carrera F. J., 2000, MNRAS, 318, 1073

Page M. J., Stevens J. A., Mittaz J. P. D., Carrera F. J., 2001a, Sci, 294, 2516

Page M. J., Mittaz J. P. D., Carrera F. J., 2001b, MNRAS, 325, 575

Page M. J., Davis S. W., Salvi N. J., 2003, MNRAS, 343, 1241

Page M. J., Stevens J. A., Ivison R. J., Carrera F. J., 2004, ApJ, 611, L85

Page M. J. et al., 2006, MNRAS, 369, 156

Pei Y. C., 1992, ApJ, 395, 130

Piconcelli E., Jiménez-Bailón E., Guainazzi M., 2004, MNRAS, 351, 161

Piconcelli E., Jiménez-Bailón E., Guainazzi M., Schartel N., Rodríguez-Pascual P. M., Santos-Lleó M., 2005, A&A, 432, 15

Porquet D., Reeves J. N., O'Brien P., Brinkmann W., 2004, A&A, 422, 85

Pounds K. A., Reeves J. N., King A. R., Page K. L., O'Brien P. T., Turner M. J. L., 2003, MNRAS, 345, 705

Reeves J. N., O'Brien P. T., Ward M. J., 2003, ApJ, 593, L65

Reeves J., Nandra K., George I. M., Pounds K. A., Turner T. J., Yaqoob T., 2004, ApJ, 602, 648

Reynolds C. S., 1997, MNRAS, 286, 513

Sako M. et al., 2003, ApJ, 596, 114

Sanders D. B., Soifer B. T., Elias J. H., Madore B. F., Matthews K., Neugebauer G., Scoville N. Z., 1988, ApJ, 325, 74

Schartel N., Rodríguez-Pascual P. M., Santos-Lleó M., Clavel J., Guainazzi M., Jiménez-Bailón E., Piconcelli E., 2005, A&A, 433, 455

Severgnini P. et al., 2000, A&A, 360, 457

Sijacki D., Springel V., di Matteo T., Hernquist L., 2007, MNRAS, 380, 877

Silk J., Rees M., 1998, A&A, 331, L1

Silverman J. D. et al., 2005, ApJ, 618, 123

Smail I., Ivison R. J., Blain A. W., 1997, ApJ, 490, L5

Steenbrugge K. et al., 2005, A&A, 434, 569

Stevens J. A., Page M. J., Ivison R. J., Carrera F. J., Mittaz J. P. D., Smail I., McHardy I. M., 2005, MNRAS, 360, 610

Strateva I. V., Brandt W. N., Schneider D. P., Vanden Berk D. E., Vignali C., 2005, AJ, 130, 387

Tolea A., Krolik J. H., Tsvetanov Z., 2002, ApJ, 578, L31

Vanden Berk D. E. et al., 2001, AJ, 122, 549

Vasudevan R. V., Fabian A. C., 2009, MNRAS, 392, 1124

Vestergaard M., 2003, ApJ, 599, 116

Vignali C., Brandt W. N., Schneider D. P., 2003, AJ, 125, 433

Waskett T. J. et al., 2003, MNRAS, 341, 1217

Wyithe J. S. B., Loeb A., 2003, ApJ, 595, 614

This paper has been typeset from a TEX/LATEX file prepared by the author.